Editors' Suggestion

Tomography of basic magnetic domain patterns in ironlike bulk material

R. Schäfer*
Leibniz Institute for Solid State and Materials Research (IFW) Dresden, Institute for Metallic Materials,
Helmholtzstrasse 20, D-01069 Dresden, Germany
and Institute for Materials Science, TU Dresden, 01062 Dresden, Germany

S. Schinnerling
Leibniz Institute for Solid State and Materials Research (IFW) Dresden, Institute for Metallic Materials,
Helmholtzstrasse 20, D-01069 Dresden, Germany

(Received 1 April 2020; revised manuscript received 28 May 2020; accepted 29 May 2020;
published 18 June 2020)

Selected magnetic domain patterns in Fe 12.8 at.% Si bulk crystals with different crystallographic surface orientation are tomographically imaged to reveal their three-dimensional structure. This alloy allows "freezing" of the domains as a precipitation pattern with subsequent imaging in a polarization microscope after cutting or successive polishing (Libovický method). The selected domain patterns are basic for materials with cubic crystal anisotropy and comprise spike, moth, fir tree, V-line, ant, chain, and echelon domains. Established domain models for these patterns are partially confirmed, but also surprising deviations and extensions of the models are found. Finally, the fundamental difference between magnetically hard- and soft-grain boundaries is revealed by combining domain tomography with surface domain observation by Kerr microscopy.

DOI: 10.1103/PhysRevB.101.214430

I. INTRODUCTION

While the full domain structure of magnetic single-layer films is easily accessible by numerous imaging techniques like Lorentz microscopy, Kerr microscopy, or x-ray spectromicroscopy (see Ref. [1] for a review), it is much more challenging to analyze the magnetic microstructure of bulk specimens in which the domains may change their appearance across the thickness or diameter. Simply cleaving a sample to look for the interior domains would be meaningless as the domains would immediately adapt to the new surface to minimize the stray field energy. To reveal the complete three-dimensional (3D) magnetization vector field experimentally, tomographic approaches are rather required, i.e., the imaging by sections or sectioning through the use of a suitable penetrating wave [2], which would leave the domains unchanged. As such possibilities were hardly available in the past, the analysis of domains in bulk, nontransparent specimens was usually performed by surface domain observation and by using arguments from domain theory to infer the inner domains [1].

In recent years, however, there was impressive progress in the development of magnetic tomographic imaging, partly triggered by advances in the fabrication of nanometer-sized three-dimensional magnetic objects with promising new functionalities [3]. Examples are as follows. (i) Domain mapping in a rolled-up, tubular magnetic film of 2-μm diameter by means of full-field *soft* x-ray spectromicroscopy [4]. (ii) The imaging of vortex structures in a soft magnetic pillar of 5-μm diameter by using *hard* x-ray tomography [5]. This method has the capability for tomography in samples with sizes of the order of tens of micrometers at a resolution around 50 nm and can even be applied in a time-resolved pump-probe mode [6]. Like soft x-ray spectromicroscopy, also hard x-ray tomography makes use of the x-ray circular magnetic dichroism effect and is thus demanding for materials with low dichroic signal at hard x-ray wavelengths, which also limits the spatial resolution. (iii) The reconstruction of the magnetization in a 60-nm diameter Co/Cu-layered nanowire with 10-nm spatial resolution by adding tomographic tools to off-axis electron holography in a transmission electron microscope [7].

In all these methods the 3D magnetization arrangement is retrieved from a set of two-dimensional (2D) projections by analyzing the evolution of magnetic contrast with varying projection angle and by using some adapted reconstruction algorithm. Nevertheless, all methods rely on the penetration of the used radiation to generate a domain contrast. Those powerful and promising tomographic techniques are therefore limited to the study of nanometer- and micrometer-sized magnetic objects, owing to penetration depths of about 200 nm in the case of soft x rays and electrons and some tens of micrometers for hard x rays. The domain anatomy of thicker, bulk materials is thus not accessible by those techniques. The same is true for conventional x-ray topography [8], which also depends on the penetration depth of hard x rays and which senses the magnetostrictive strain connected with a domain pattern. Therefore only domains that are magnetized along different axes in otherwise perfect crystals [1] can be indirectly seen [9], which strongly limits the method.

Tomography of domains in "true" bulk specimens became reality in the past decade with the introduction of neutron dark field microscopy [10]. This method is based on small-angle scattering of neutrons at magnetic domain walls that

---

[*] Corresponding author: r.schaefer@ifw-dresden.de

has a detectable influence on the spatial coherence of the neutron wave front. It allows to visualize the internal domain structure on a wide variety of specimens with thicknesses of several millimeters and is well suited for investigating materials under the influence of external parameters like magnetic field, temperature, or stress. Also time-resolved, stroboscopic microscopy at power frequency was demonstrated on grain-oriented electrical steel sheets [11]. In 2010, Manke *et al.* [12] modified the experimental arrangement and achieved the first 3D mapping of the magnetic domains in the bulk of an iron-silicon crystal with a thickness of 8 mm. Neutron dark-field tomography suffers, however, from a low spatial resolution that is limited to lengthscales of the order of tens of micrometres at best and from the fact that just the location of domain walls can be imaged rather than the domain magnetization itself. So, in the impressive domain tomogram of Ref. [12] only the 3D network of domain walls within the *bulk* could be seen, while the finer, multiply branched domains within a depth of about 50 μm from the surface could not be resolved thus providing only a incomplete picture of the domain anatomy.

So the previously listed magnetic tomography methods have restrictions, either in terms of spatial resolution, allowed specimen thickness, or "size" and thus the availability and cost of the required equipment (needed are advanced electron microscopes, synchrotrons, or neutron sources). Common to them, however, is the advantage of being nondestructive. In 1972, already, a unique but *destructive* tomographic method for 3D domain imaging was discovered by Libovický [13]. He found that a Fe 12.8 at.% Si alloy precipitates submicroscopic platelets with a DO_3 ordered crystal structure that grow inside the matrix with B_2 structure when annealed at about 580° C (above a eutectic line [14] at 540° C, see Fig. 1(a)). As the annealing temperature is below the Curie point, both, precipitates and matrix are still ferromagnetic and the material (magnetically) behaves like a homogeneous ferromagnet during annealing. It actually contains magnetic domains that resemble those of iron with a positive cubic magnetocrystalline anisotropy. Those platelets [Fig. 1(b)], which are formed throughout the specimen, are oriented along the {100} planes of the cubic crystal for energetic reasons, and by some magnetostrictive interaction [13] they are preferably aligned along the local magnetization direction as schematically shown in Fig. 1(c). The platelet texture thus resembles the domain pattern present at the reaction temperature. After cooling down to room temperature, the high-temperature domain structure remains then "frozen" as a precipitation pattern. The precipitation texture gives rise to a birefringence effect after etching, which leads to an areal domain contrast in an optical polarization microscope. All three magnetization axes can be distinguished and at high magnification even domain walls can be seen. The volume structure of the frozen-in domain pattern is then revealed by successively polishing away the surface or by cutting the sample.

The Libovický method is limited to the very specific FeSi alloy with a silicon content around 13 at.%, it is destructive and it permits only a one-time investigation of domains that were present at the annealing temperature of 580° C. Nevertheless, it has the unique potential to reveal the full anatomy of a complex domain state in an arbitrarily thick poly or single crystal with a high resolution in the micrometer range. Compared to pure iron at room temperature, the magnetic energies that determine the domain character will, in detail, be different for the FeSi alloy at elevated temperature. The "frozen" domains of this material are nonetheless of the same *basic character* as in iron, thus resembling those of any other ironlike material with positive cubic magnetocrystalline anisotropy, including the typical Fe 3 wt% Si electrical steel material. This grants a more general relevance to the Libovický method to fundamental domain research.

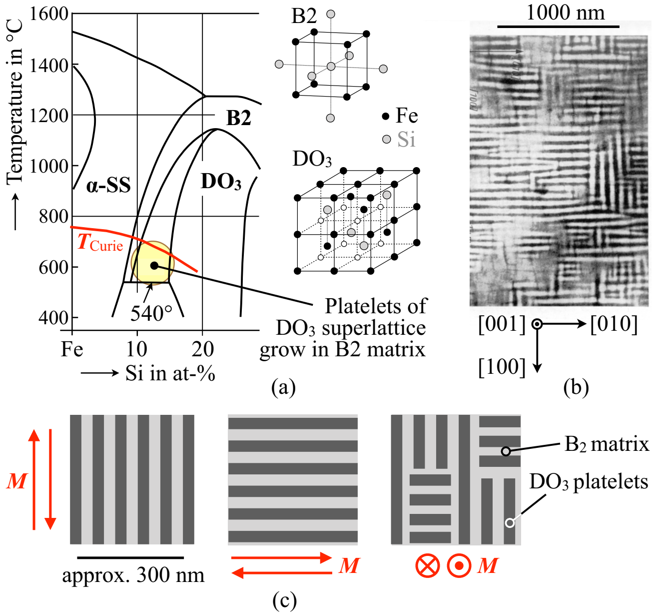

FIG. 1. Basics of Libovický's method of domain tomography. (a) Phase diagram of the Fe-Si alloy, schematically traced after Ref. [14]. Highlighted is the area in which submicroscopic precipitates with DO_3 crystal structure grow in a B2 matrix at annealing. (b) Transmission electron micrograph of the precipitates after annealing a Fe 12.8 at.% Si crystal for 70 hours at 580° C, reprinted by permission from Ref. [13]. (**c**) Schematics of the magnetization-dependent platelet texture. The platelets are aligned along one of the three {100} planes of the crystal with a preference of the plane that is also occupied by the magnetization vector (note that at the annealing temperature the FeSi alloy has a positive cubic magnetocrystalline anisotropy with the ⟨100⟩ axes being the easy axes for the magnetization).

Although being so powerful, it took some 30 years till the Libovický method was revived [15] after its first demonstration. In Ref. [16] it was applied to a silicon iron crystal with (111) principal surfaces and a thickness of 1 mm. The validity of a three-dimensional echelon model for domain refinement close to such extremely misoriented surfaces was verified for the first time (in Sec. III G of this paper we will address that pattern again and evaluate it quantitatively). Later [17], Libovický tomography was applied to study the domain structure in a crystal with slightly misoriented (110) surface, resembling the typical orientation of Goss-textured electrical transformer steel. A 3D domain anatomy that was more complicated than expected from theory was revealed by serial sectioning, most likely caused by the influence of mechanical stress (see Supplemental Material [18]).

This article is devoted to a number of selected domain patterns, which are well known for iron and that are discussed in the textbook *Magnetic Domains* [1]. They comprise spike, moth, fir tree, V-line, ant, chain, and echelon domains. By Libovický tomography their 3D anatomy is experimentally studied to proof domain models, which were previously derived from surface domain observation and by using arguments from domain theory. At the end we will also address grain boundary domains, showing that Libovický studies deserve further attention to analyze the role of grain boundaries for flux propagation in polycrystalline bulk materials like electrical steel.

II. EXPERIMENT

A Fe 12.8 at.% Si single crystal with a length of 40 mm and a diameter of 6 mm was grown by zone melting. On approaching the end of the crystal, monocrystallinity was lost so that also a polycrystalline specimen with grain sizes in the millimeter range was available. Disks with typically 1-mm thickness and selected crystallographic surface orientations (determined by radiography) were cut from the crystal by using an electro-erosive saw to avoid damage of the cut faces. The disks were then manually ground and polished from both sides to generate plane-parallel principal surfaces. For final polishing, a colloidal suspension of amorphous SiO_2 particles [OP-S® (Struers)] was used which provides combined chemical and mechanical material removal leading to stress-free surfaces. For the studies in Sec. III G wedge-shaped crystals with (111) surfaces and different slopes were prepared and treated accordingly.

For annealing in a ceramic tube furnace, the samples were sealed in quartz glass ampoules at a vacuum of 10^{-3} Pa with a tantalum sheet added as getter material. The ampoules were surrounded by an iron shielding to prevent effects from magnetic fields during annealing. After two hours homogenization annealing at 1140° C, the specimens were cooled below the Curie temperature and then held at 580° C for 60 hours to execute the precipitation reaction. After cooling to room temperature the crystals were ready for tomography.

To reveal the volume domains, an annealed crystal was either erosively cut along specific planes or the surface of the specimen was removed in defined steps and the domain anatomy was then displayed along selectable cross sections after combining the images in a tomography computer program (AMIRA-AVIZO® and DIGITALMICROGRAPH® Software). For the second situation, an OP-S-based nanopolishing procedure was applied with the sample clamped in an Accustop® (Struers) specimen holder. Manual polishing of 2.5 minutes resulted in the removal of 0.5 μm which was the finest, reproducible step size. After each polishing step the surface was etched to reveal the precipitation pattern of the "frozen" domains in the polarization microscope. Different to Libovický, who used electrolytic etching [13], we applied a normal iron etchant (2% Nital, 15 s) that produced more homogeneous etching results. More details on preparation can be found in Ref. [15].

Domain imaging was finally performed in an optical polarization microscope that was originally optimized for Kerr microscopy [19]. The domain contrast after etching a precipitated iron-silicon crystal is due to an optical birefringence effect that is caused by the precipitation texture. It has a similar contrast symmetry as the magneto-optical Voigt effect (linear magnetic birefringence [20]), i.e., the domains show up in an areal contrast, which depends quadratically on the magnetization and which changes sign by rotating the sample by 90°. Antiparallel domains thus show up in the same color, but they can easily be distinguished as the 180° domain wall, separating them, can be resolved by using high-resolution objective lenses. The domain contrast is strongest at crossed polarizers and it can be optimized and inverted by opening a rotatable compensator (a quarter wave plate in our case). A thorough Libovický-contrast analysis was performed in Ref. [16].

III. RESULTS

At zero and low applied magnetic field, the principal of domain formation in ironlike material is the avoidance of magnetic poles, best by properly arranged domains that are magnetized along the easy $\langle 100\rangle$ axes to avoid anisotropy energy [1]. Both conditions can easily be fulfilled if a crystal surface contains one or two easy axes, which is the case for ideally oriented $\{100\}$ and $\{110\}$ surfaces. For misoriented surfaces, supplementary domain patterns or branched structures [1] are formed to meet those requirements as well as possible.

In the following subsections the 3D structures of selected domain patterns, which follow that basic principle, are presented. To introduce the patterns, we first show Kerr micrographs or model sketches in each case, which are mostly reprinted from the monograph *Magnetic Domains* [1], followed by Libovický observations.

A. Néel spikes

In materials with cubic magnetocrystalline anisotropy there are multiple easy directions for the magnetization, which leads to a much larger variety of possible domain states as compared to materials with just a single easy axis as they are requirement for permanent magnets. In the case of iron (and our FeSi alloy) these are the mentioned six $\langle 100\rangle$ directions of the cubic elementary cell. In 1944, Néel [21] made use of these possibilities and predicted a spike domain state that forms around large nonmagnetic inclusions or holes in iron crystals [Fig. 2(a)]. Those *Néel spikes*, which purely consist of easy-axis domains, guide the magnetic flux around the defect to avoid magnetic poles that would otherwise be present around the defect. A few years later the spikes were indeed discovered by Bitter imaging [22] and identified as a source of Barkhausen jumps and coercivity [23]. In Figs. 2(b) and 2(c) this effect is demonstrated for a hole in an iron film: The 180° wall, approaching the defect from the top in an applied field, is "caught" by the *Néel spikes* and pinned to the defect.

In the past, Néel spikes were exclusively studied by surface domain observation (see, e.g., Refs. [24–26]). Here, we report that they can also exist — not unexpectedly — in the volume

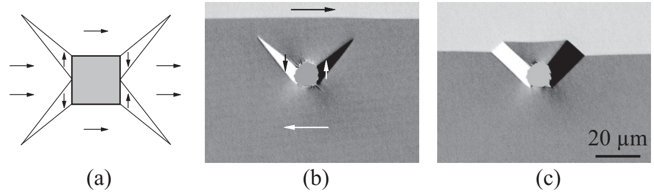

FIG. 2. (a) Schematics of a Néel spike that guides the magnetic flux around a large nonmagnetic defect in iron. In (b, c) such spikes and their effect on a 180° domain wall is visualized by Kerr microscopy on a 100-nm-thick iron film in (100) orientation. All images are reprinted by permission from *Magnetic Domains* [1].

of a crystal. As shown in Fig. 3, we found a 10-μm large pore at a depth of approximately 50-μm away from the surface of an annealed FeSi Libovický crystal. The frozen domains around the defect reveal the spikes that tie a 180° wall to the defect. On polishing down in micrometer steps it becomes evident that also the 90° domain wall on the right side in the images is linked to the hole, proving that such defects can have effects on the whole domain wall network in their neighborhood.

B. Fir tree pattern

The fir tree pattern is found on a (100)-related surface of ironlike material if one or two of the easy axes are slightly misoriented by some degrees. There are two types of such patterns, depending on the character of the basic domain walls as shown schematically in Fig. 4 together with Kerr micrographs. In each case the shallow fir tree domains at the surface collect the magnetic flux, which is guided towards a misoriented surface within the basic domains, and distribute it to a neighboring basic domain. According to the models, the fir tree branches are restricted to the surface region in both cases, while in the volume much wider basic domains are expected. The effective reduction of the surface domain width reduces the stray field energy, while at the same time some domain wall energy is saved by allowing for wide volume domains. Because this system of compensating domains is superimposed on the basic domains, the fir trees belong to the category of so-called *supplementary domains* [1].

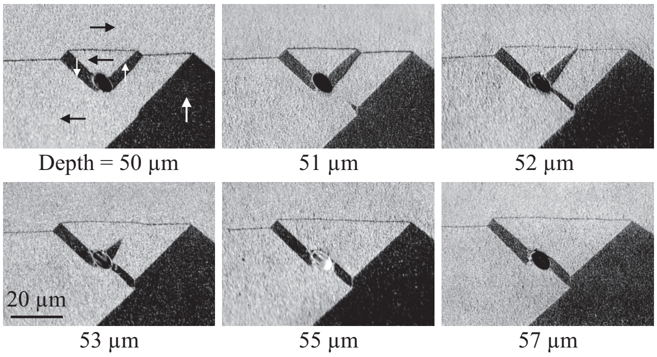

FIG. 3. Frozen domains around a defect that was found after removing 50 μm of material in a precipitated FeSi crystal with (100) surface. In the course of the images the sample was polished in micrometer steps as indicated.

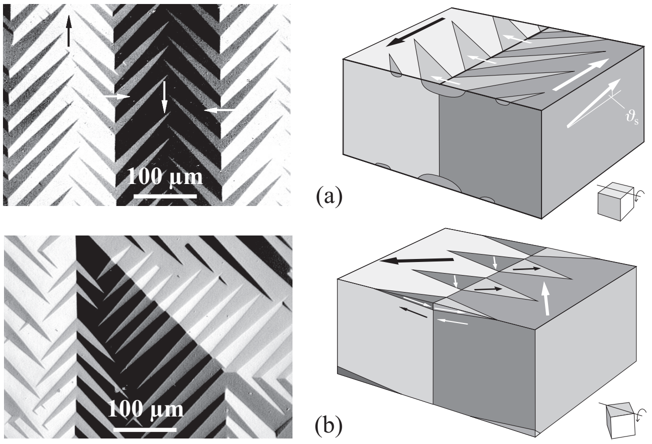

FIG. 4. Two variants of the fir tree pattern, associated with 180° basic domain walls in (a) and with a 90° wall in (b). The Kerr images are from the surface of a slightly misoriented, (100)-related surface of a Fe 3 wt% Si sheet with a thickness of 0.5 μm. All images are reprinted by permission from *Magnetic Domains* [1].

On a polycrystalline FeSi specimen we were able to identify a large (100)-related grain with frozen fir tree domains (Fig. 5). For tomography, the crystal was polished in steps down to a depth of 68 μm to reveal the underlying volume domain structure. In Fig. 5(a) the stack of images is displayed perspectively and in Figs. 5(b) to 5(e) the domain states at various depths are shown. As expected, the fir tree branches are indeed surface domains that disappear in a depth around 10 μm. In the main grain, an array of 180° walls shows up then [Fig. 5(b)], most of them being truncated by round domain walls to form "tongue"-shaped domains. With increasing depth the tongues continuously withdraw [Figs. 5(c) and 5(d)] till they finally disappear at a depth of 55 μm [Fig. 5(e)].

The side views in Fig. 6, which were obtained by "cutting" the stack of images in the computer, reveal the anatomy of the domains. Cuts (A) and (B) were taken across fir tree branches that are associated with 180° basic domain walls, proving that those branches are indeed shallow surface domains as expected from the domain model [Fig. 4(a)]. The same is true for the fir tree branch associated with a 90° wall [Cut (C)], which also verifies the corresponding model [Fig. 4(b)]. Cut (D) reveals a 180° domain wall from which a misorientation of 6° can be derived. Together with Cut (B) it furthermore indicates that the fir trees in that sample area are attached to basic 180° walls, which do not proceed towards the depth according to the model in Fig. 4(a), but which rather bend around to form the mentioned tongue-shaped domains.

As schematically shown in Fig. 7(a), those tongues are shallow surface domains, similar to the lancet domains in the lancet comb pattern [Fig. 7(b)] that is found on slightly misoriented (110)-surfaces [1]. In the second of these the magnetic flux, guided towards the top surface by a basic [001]-domain, is collected by the lancet comb and returned to the bottom surface by a common internal, transverse [100]- or [010]-domain. In the case of the tongue pattern on the [100]-related surface [Fig. 7(a)], flux distribution is possible by

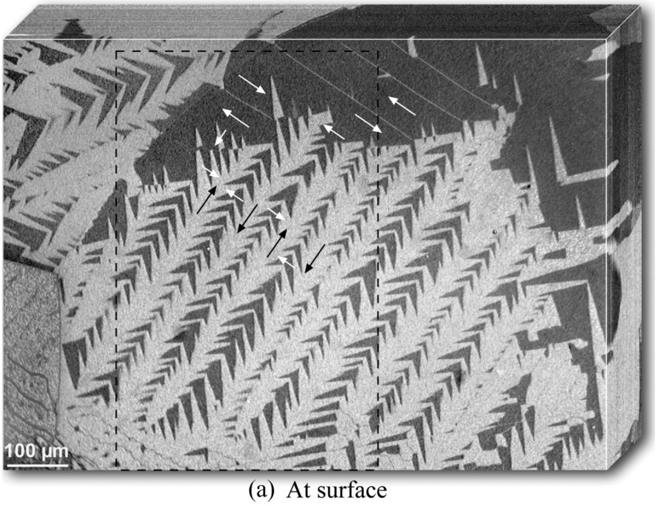

(a) At surface

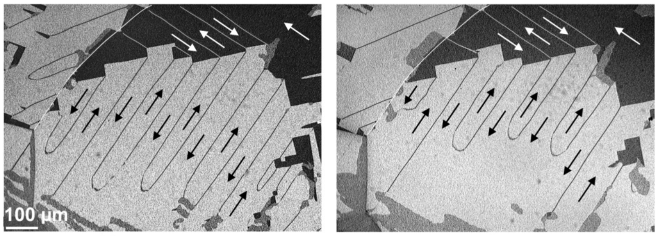

(b) At 11 µm (c) At 27 µm

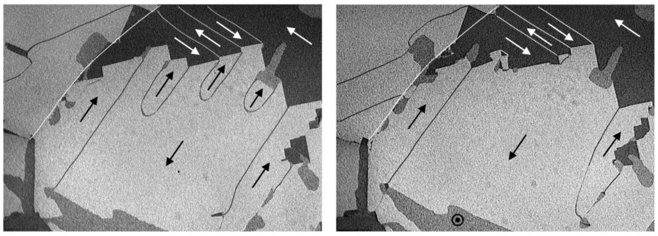

(d) At 40 µm (e) At 55 µm

FIG. 5. Frozen fir tree domains in a FeSi Libovický crystal with slightly misoriented (100) main surface. The surface was polished in steps of 0.5 μm down to a depth of 18 μm and then further in steps of 1 μm down to 68 μm depth. The 87 slices were superimposed in a tomographic computer program and displayed in a perspective view in (a). The dashed frame indicates the area that was selected for Fig. 6. In (b) to (e) the domains in various depths as indicated are shown in reduced size. Here the domain walls were traced by lines to enhance their visibility. For the complete collage of unprocessed images we refer to the Supplemental Material [27].

domains that are magnetized along the perpendicular [001]- or transverse [010]-axes as visible on the left or right sides of Cut (D) in Fig. 6.

The tongue domains may be seen as a first-generation supplementary domain pattern, on which the fir trees as a second-generation pattern are superimposed. This possibility of multigeneration supplementary domains for an effective reduction of stray field energy on slightly misoriented {100}-related surfaces was apparently overlooked in the past.

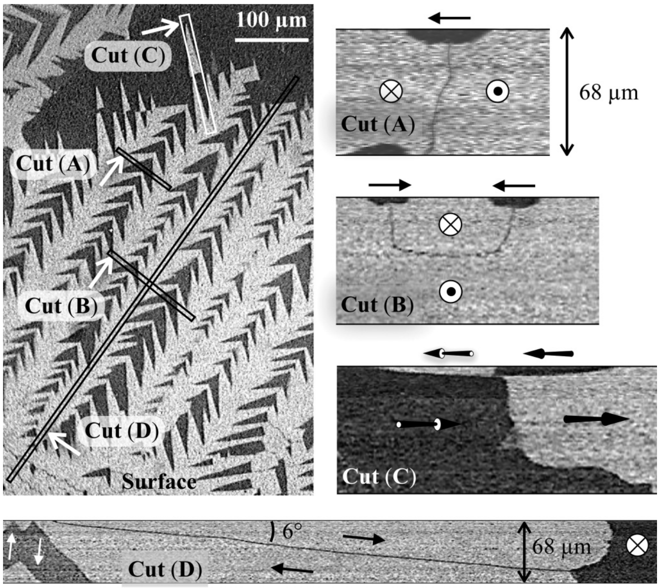

FIG. 6. Frozen fir tree domains in the area that was marked by the dashed frame in Fig. 5(a) together with cross-sectional cuts perpendicular to the surface. The narrow frames in the main figure indicate the planes of the cuts and the arrows the viewing directions

C. V-line pattern

If in an ironlike crystal with (100)-related surface the easy axis perpendicular to the surface is occupied in the bulk, possibly favored by magnetostrictive interaction due to mechanical stress, closure domains are formed at the surface as shown in Fig. 8(a). The 90° domain walls, which separate the closure and basic domains, are zigzag folded to lower their specific energy [1]. The intersections of these walls at the surface, visible by Kerr microscopy [Fig. 8(b)], are characterized by head-on configurations of the surface magnetization. For their V-shaped internal structure they are called V-lines.

By Libovický tomography the V-line model can be proven. The top and side views on an ideally oriented (100) crystal [Fig. 8(c)] reveal the closure domains with zigzag walls and the underlying perpendicular domains. Interestingly, the

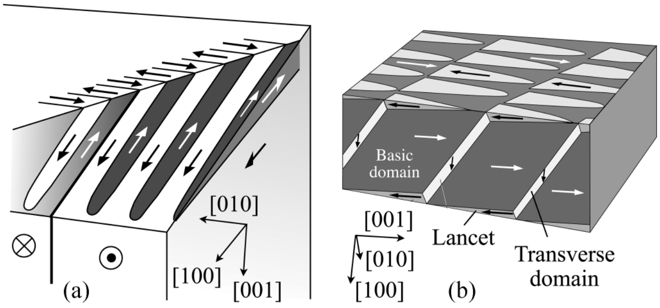

FIG. 7. (a) Schematic representation of a two-generation supplementary domain structure on a slightly misoriented {100}-related surface. Shown is the first-generation pattern in top and side views, which consists of a row of shallow surface domains in the shape of tongues on which the second-generation fir trees (not shown) are superimposed. In (b) the lancet comb pattern, occurring on a lightly misoriented {110}-related surface, is shown for comparison. The model drawing in (b) is reprinted by permission from *Magnetic Domains* [1].

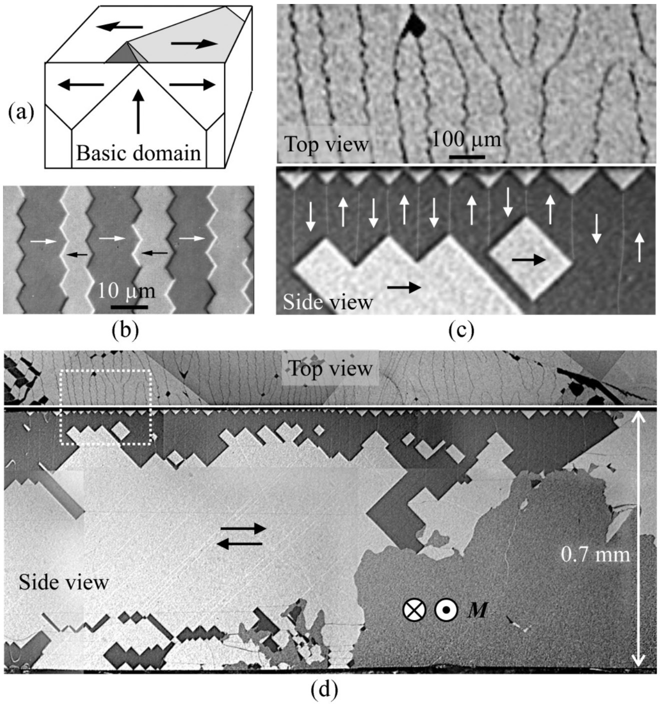

FIG. 8. (a) V-line model for an ironlike crystal with (100) surface, in which the perpendicular easy axis is favored by a planar compressive stress (under the assumption of positive magnetostriction). (b) Kerr micrograph of zigzag walls at the surface intersection of the closure domains, imaged on a 0.5-mm-thick Fe 3 wt% Si electrical steel sheet. (c) "Frozen" V-line pattern in a Libovický crystal, seen from the top and on a (010) cross section perpendicular to the surface. (d) Top view and cross section across the whole crystal thickness. The area, selected in (c), is marked by a frame. Images (a) and (b) are adapted by permission from *Magnetic Domains* [1].

V-line pattern is restricted to a surface zone as can be seen by looking at the complete cross section of the 0.7-mm-thick FeSi crystal [Fig. 8(d)]. Such a *layered* domain character can not easily be derived from surface observations alone. Locally varying mechanical stress, which leads to a local preference of one of the three crystallographic easy axes relative to the others by magnetostrictive interaction, may be a reason [18]. Layered domains seem to be a very general phenomena in bulk crystals — a further example will be shown in Sec. III G.

D. Moth pattern

If a V-line pattern is enforced at a slightly misoriented (100) surface, magnetic poles would be created at the surface of the closure domains under the assumption that the magnetization follows the easy axes [see inset in Fig. 9(a)]. The related stray field energy is then reduced by superimposed supplementary domains that resemble moths and butterflies if imaged by Kerr microscopy [Fig. 9(a)]. They collect the magnetic flux that is guided towards the surface and distribute it back to the volume. The head-on and head-on-side magnetization configuration at their "tails," highlighted in the top view of Fig. 9(b), indicate that these tail walls are actually V-lines. In Chap. 5.3.4 of *Magnetic Domains* [1] their function is described as follows: "Note the V-lines at the tails of the "butterflies" and "moths," which indicate that the collected flux is transported into the interior, towards the basic domains...". This principle is illustrated in the side view diagram of Fig. 9(b).

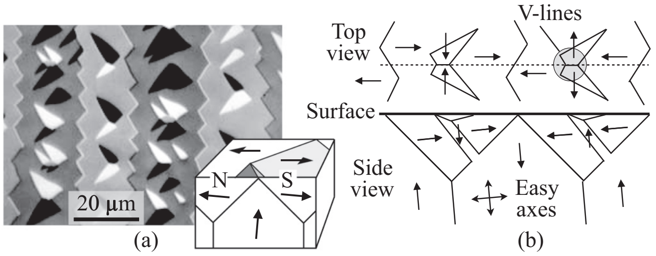

FIG. 9. (a) Butterfly and moth domains, imaged by Kerr microscopy on the surface of a slightly misoriented, (100)-related surface of a Fe3wt%Si sheet with a thickness of 0.5 mm. The inset shows the V-line model for the case of slight misorientation with magnetic poles indicated. (b) Schematics of top and side views according to conventional understanding. The side view is taken along the dashed line in the top view. The Kerr image is reprinted by permission from *Magnetic Domains* [1].

Our bulk domain analysis, however, reveals a different mechanism. In Fig. 10(a) a perspective view of a frozen moth pattern is shown. Like for Fig. 5(a) it was obtained by successive polishing in steps and by superimposing the Libovický images in the computer. Immediately evident is the closure structure of the surface domains and the zigzag folding of the V-lines, both expected from the V-line model [Fig. 8(a) and inset in Fig. 9(a)]. The cross-sectional cut in Fig. 10(b) reveals the internal domain that is connected to the tail of a moth domain. According to the model in Fig. 9(b), it would be expected that this domain proceeds towards the right to allow flux transport to or away from the perpendicular basic domains. Surprisingly, however, that domain is inclined to the left, thus suggesting the model sketched in Fig. 10(c). Apparently, the magnetic flux, collected by the moth domains at the surface, is not directed to the inner basic domains as assumed. It is rather kept within the closure domains, all achieved by pole-free 90° domain walls. This "left-alignment" of the subsurface domains applies to all moths as can be verified by following the domain development towards the depth in the videos "Moth" in the Supplemental Material [28].

We may therefore conclude that on slightly misoriented, (100)-related surfaces in ironlike material the supplementary domains are always restricted to the surface zone. This is possible due to the existence of two (almost) surface-parallel easy axes that allow flux guidance along the surface, possibly supported by some near-surface internal domains as in the butterfly/moth pattern. Different conditions apply to slightly misoriented, (110)-related surfaces. Here there is only one (almost) surface-parallel easy axis. The lancet domains, collecting the flux at the surface, are always connected to internal domains that guide the flux either through the bulk to the opposite surface [like in Fig. 7(b)] or along the bulk to a neighboring basic domain [1]. Flux transport throughout the bulk my also be *enforced* for the case of a (100) related surface with fir tree domains, if in an applied magnetic field one type of the basic domains, to which the flux is normally

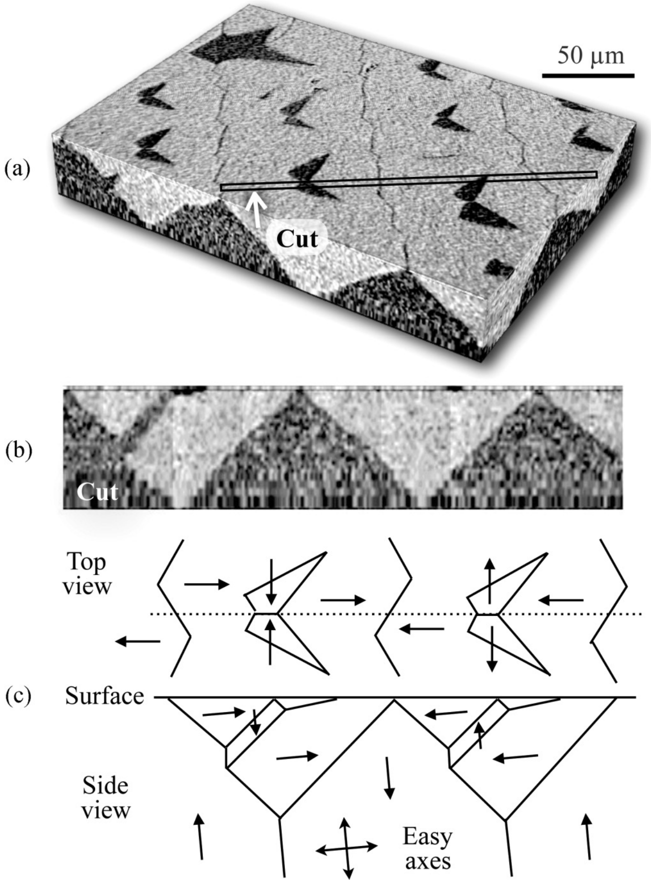

FIG. 10. (a) Frozen moth domains on a slightly misoriented Libovický crystal, displayed in a perspective view. The surface was polished in steps of 1 μm down to a depth of 22 μm and then further in steps of some micrometers down to 48 μm depth, and like in Fig. 5(a) the 33 slices were superimposed in a tomographic computer program. (b) Cross-sectional cut perpendicular to the surface along the frame indicated in (a). The model in (c) was derived from the side view under the assumption of pole-free domain wall orientations. For a complete collage of the domain images in (a) we refer to the Supplemental Material [28].

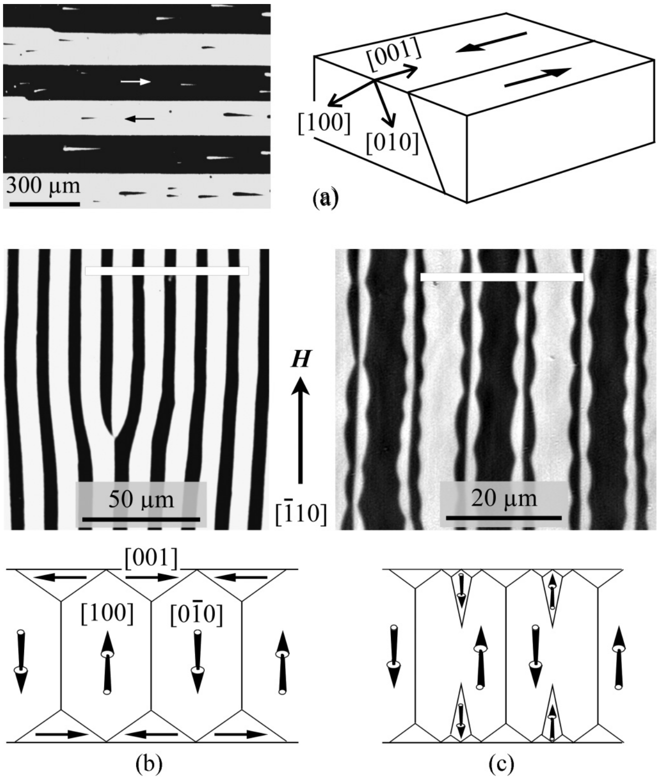

FIG. 11. (a) Basic domain state of an ironlike crystal with (110) surface, shown here by Kerr microscopy on a Fe3wt%Si sheet with a thickness of 0.3 mm. In a magnetic field transverse to the surface-parallel easy axis the column pattern (b) is enforced, which develops a branched structure (c) with a "chainlike" appearance beyond some critical field. The models represent cross-sections through the patterns as indicated in the Kerr micrographs. The images are reprinted by permission from *Magnetic Domains* [1].

guided along the surface, is eliminated. Fir tree patterns with pronounced "trunks" are then generated (see Chap. 3.7.1C in *Magnetic Domainss* [1]).

E. Chain pattern

The magnetic ground state of an ideally oriented crystal with (110) surface consists of 180° basic domains that are magnetized along the surface-parallel easy axis [Fig. 11(a)]. This is the typical domain state of Goss-textured electrical steel sheets, possibly being superimposed by some lancets in case of slight misorientation [1]. In an applied magnetic field along the [$\bar{1}$10] direction (i.e., transverse to the [001] direction), magnetic flux needs to be transported along the field direction. This is achieved by volume domains that are magnetized along the easy [100] and [0$\bar{1}$0] directions, leading to the so-called column pattern [1] [Fig. 11(b)]. In a stronger transverse field the outermost closure domains, which are magnetized transverse to the field direction, become unfavorable. Beyond some critical field the column pattern then transforms into the branched structure shown in Fig. 11(c). Here the closure volume is reduced on the expense of spike domains, which add to the domain volume magnetized along the [100] and [0$\bar{1}$0] directions like the basic domains. On the surface the closure domains of that branched structure develop a chainlike appearance.

By coincidence we discovered a chain pattern on the (100) surface of a Libovický crystal [Fig. 12(a)] although the FeSi crystal was annealed in the absence of a field. It rather seems that mechanical stress during annealing favored the internal easy axes, possibly supported by some domain topology in the surrounding neighborhood that created an effective internal field. Anyway, after mechanically cutting the crystal perpendicular to the surface, a spike and closure domain structure is revealed [Fig. 12(b)] that exactly resembles the prediction of the (intuitive) model shown in Fig. 11(c).

F. Ant pattern

A compressive stress along the preferred [001] easy axis on a (110) oriented ironlike material leads to a preference of the internal [100] or [010] easy axes for magnetostrictive reasons [for the directions, compare Fig. 11(a)]. Closure domains are then formed at the surface similar to those of the

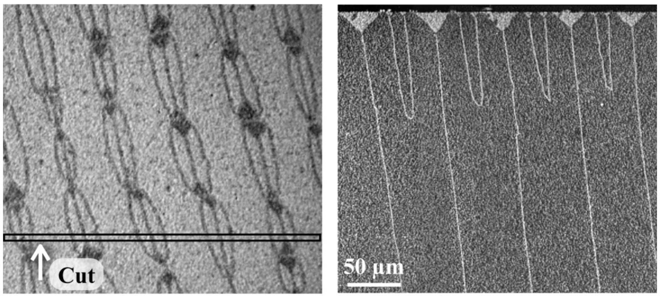

(a) Surface (b) Side view

FIG. 12. Frozen chain domains in an annealed Libovický crystal, shown in top view (a) and from the side (b) after mechanically cutting the crystal along a similar line as indicated in (a). The revealed domain anatomy confirms the model of Fig. 11(c).

column pattern shown in Fig. 11(b) (note the difference: in the column pattern the basic domains are separated by 90° domain walls while in the stress pattern they are separated by 180° walls — see *Magnetic Domains* [1] for details). At stronger pressure the closure domains are subdivided, leading to a branched pattern known as stress pattern II [1]. If imaged by Kerr microscopy under conditions that mainly the domain walls show up as contrast, those domains resemble "ants" as prominently visualized in Fig. 13(a). The model in Fig. 13(b) gives an idea about the complexity of this pattern. It turns out that only the shallow surface domains are magnetized along the surface-parallel easy axis, which is actually disfavored by the stress. The intermediate subsurface domains, which connect the closure domains with the 180° basic domains, are all magnetized along the internal easy axes that are favored by the stress.

Anyway, according to the model it is expected that the ants and their complex subsurface domains are confined to the surface neighborhood, while wide and simple basic domains should be present underneath. The Libovický analysis in Fig. 14 confirms this model. When polishing a (110) surface with frozen-in ant domains in steps, the domain complexity indeed disappears already at a depth of about 3 μm. In the images at 3 and 10 μm depth the basic domain walls are faintly seen as white lines in the otherwise dark background contrast.

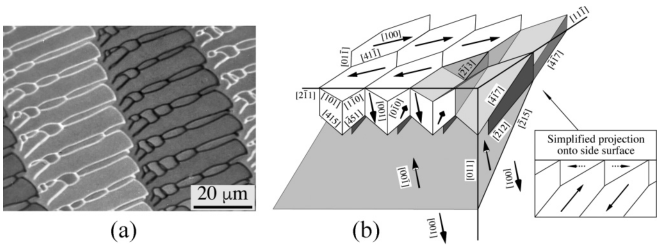

(a) (b)

FIG. 13. (a) Kerr micrograph of stress pattern II on the (110) surface of an Fe3wt%Si sheet with 0.3-mm thickness, imaged under conditions that reveal domain wall contrast. The model in (b) gives an impression of the domain complexity in the neighbourhood of the surface. All images are reprinted by permission from *Magnetic Domains* [1].

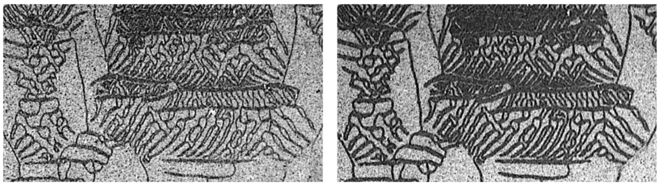

Depth: 0.25 µm Depth: 0.50 µm

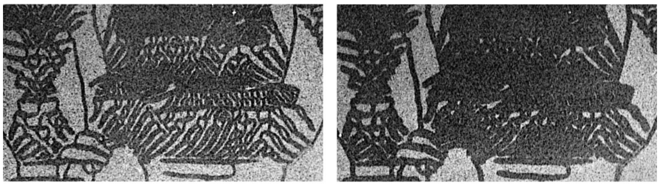

Depth: 0.75 µm Depth: 1.25 µm

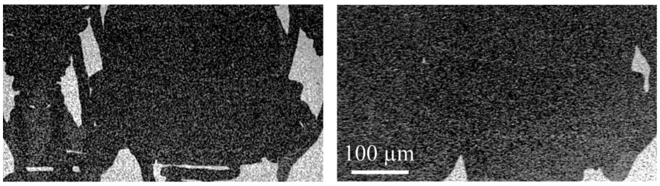

Depth: 3.00 µm Depth: 10.00 µm

FIG. 14. Ant domains on the (110) surface of an annealed Libovický crystal, and their disappearance towards the depth. For a comprehensive collection of domain images at various depths we refer to Supplemental Material [29].

G. Echelon pattern

For ironlike material with (111) main surfaces, the two requirements for domain formation — the avoidance of magnetic poles by easy axis domains — are incompatible. Here the easy axes are at an angle of 36° to the surface, which is the maximum possible misorientation angle. As sketched in Fig. 15(a), all domains can follow the easy axes in the bulk, thus avoiding anisotropy energy, while at the surface closure domains with in-plane magnetization need to be formed to avoid poles. Although anisotropy energy is connected to the closure domains, such a domain state can nevertheless be found in *thin* (111) crystals [12].

With increasing sample thickness, however, the basic domain width increases [compare Fig. 15(e)] and with it the size of the unfavorable closure domains. To keep the anisotropy energy of the closure domains low, their volume has to shrink. Beyond some critical sample thickness this is achieved by the formation of the echelon pattern [Fig. 15(c)], a branched structure in which the domain width is progressively reduced towards the surface in a two-dimensional, stray-field-free manner. All subsurface domains are easy axes domains, avoiding anisotropy energy, while the volume of the outermost, hard-axis closure domains is reduced. With further increasing crystal thickness the echelon pattern is iterated using two generations of refinement [Fig. 15(d)] and more (not shown) with rising thickness. With this branching scheme the closure volume is kept small while at the same time domain wall energy is saved by keeping the basic domains wide. The multiple generations of the underlying echelons can indirectly be seen by Kerr microscopy, which images the outermost closure domains [Fig. 15(b)].

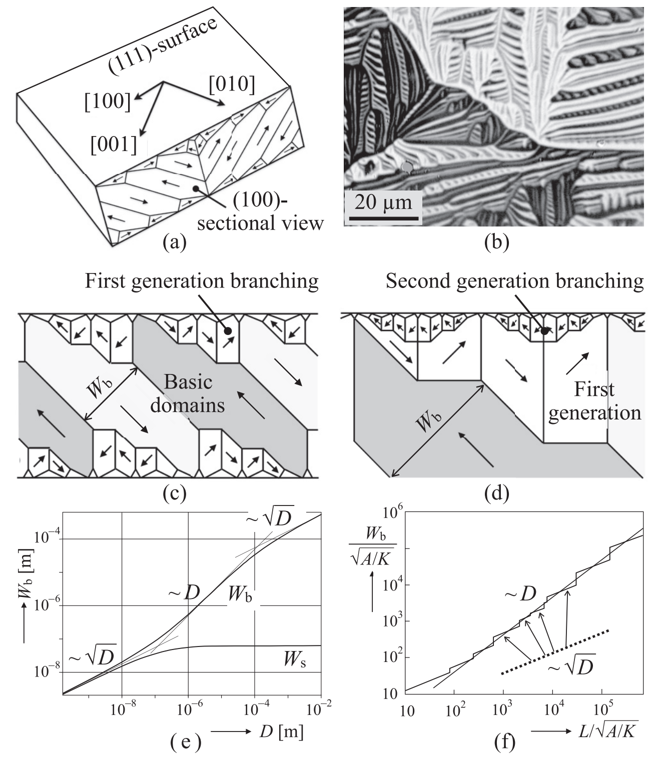

FIG. 15. (a) Fundamental domain structure in an ironlike crystal with (111) surface as seen along a (100) cross-section plane. Domains along the (100) easy axis are ignored for simplicity. (b) Kerr micrograph on the (111) surface of a 0.2-mm-thick Fe 12.8 at.% Si crystal before Libovický annealing. (c) First generation- and (d) second generation echelon pattern. (e) Bulk domain width W_b and surface width W_s as a function of crystal thickness D with indication of the three characteristic regimes. (f) Basic domain width as a function of thickness in the linear regime, showing that the overall linear dependency is actually an average over square root steps. The schematics are taken from Ref. [12], the graphs are reprinted by permission from *Magnetic Domains* [1].

By domain theory [1] [Fig. 15(e)] a $W_b \sim \sqrt{D}$ dependency of the basic domain width W_b is found for small thickness D, which then changes to a $W_b \sim D$ dependency when multiple generations of echelons are added with rising thickness, bending to a square root dependence again at very large thickness where no further generations are added. At the same time the surface domain width remains constant and independent of the complexity of the interior domains. In Ref. [12] the curve predicted in Fig. 15(e) could be proven experimentally by combining Kerr and neutron imaging on a wedge-shaped FeSi-crystal. In that work we made use of the fact that the "life" volume domains can be indirectly seen at the surface by a superstructure contrast that is superimposed to the fine closure domain contrast — in the Kerr image in Fig. 15(b) two such volume domains can be attributed to the bright and dark areas in the upper right and lower left halves, respectively. Up to crystal thicknesses of some 100 μm the superstructures can be ordered after proper demagnetisation treatment, allowing to deduce the volume domain width quantitatively. For larger thickness the domains were sufficiently wide to be resolved by neutron tomography.

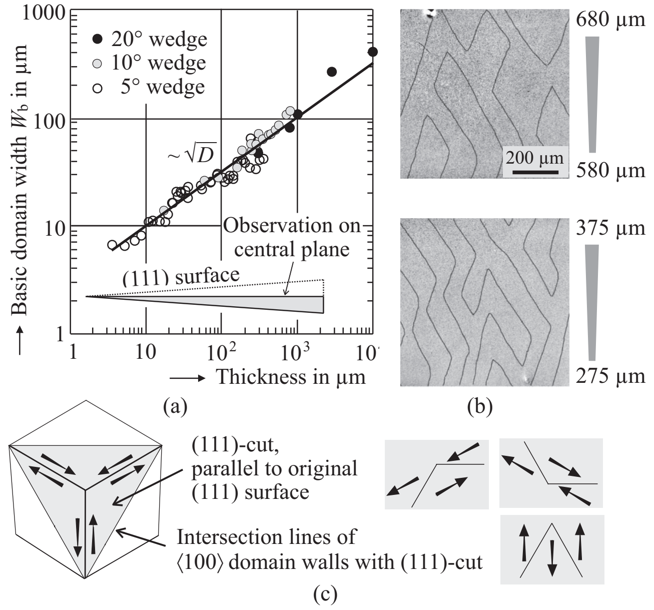

FIG. 16. (a) "Frozen" basic domain width as a function of crystal thickness, measured on the central planes of three wedge samples after cutting the wedges as indicated. (b) Typical 180° wall configurations on the central plane for two thickness ranges and (c) explanation of the possible wall angles.

To verify the model by Libovický studies we prepared three wedge-shaped crystals with (111) surface, wedge angles of 5°, 10°, and 20° and lengths of some millimetres each. After annealing, the wedges were cut by half and the "frozen" domains were imaged on the central plane as indicated in the inset of Fig. 16(a). On that plane usually large areas of homogeneous color show up in which, under the given contrast conditions, only the intersections of 180° domain walls are seen as a line contrast. Two typical examples at two thickness ranges are shown in Fig. 16(b). According to the schematics in Fig. 16(c), the 180° walls can intersect the central plane, which is approximately parallel to the original (111) surface, at three defined angles — two of them can be identified in the images in Fig. 16(b). The wall distance corresponds to the domain width in the center of the wedge specimens, which can now be evaluated as a function of wedge thickness.

In Fig. 16(a) the bulk domain width W_b is plotted as a function of the crystal thickness D for three and a half orders of thickness. Interestingly, the domain width follows a square root law over the entire evaluable thickness range. The expected linear range according to Fig. 15(e) is obviously not found in the frozen domain pattern. This finding, however, is not in contradiction to theory. According to theory [1], a $W_b \sim D$ dependence is expected if with increasing thickness more and more generations of echelons are added as shown in Fig. 15(f). Within one generation, however, the slope follows a $W_b \sim \sqrt{D}$ dependency. This the case for our Libovický crystals. As can be seen along the (100) cross sectional plane of a crystal with (111) surface and constant thickness [Fig. 17(a)], the echelons in our material are not iterated but

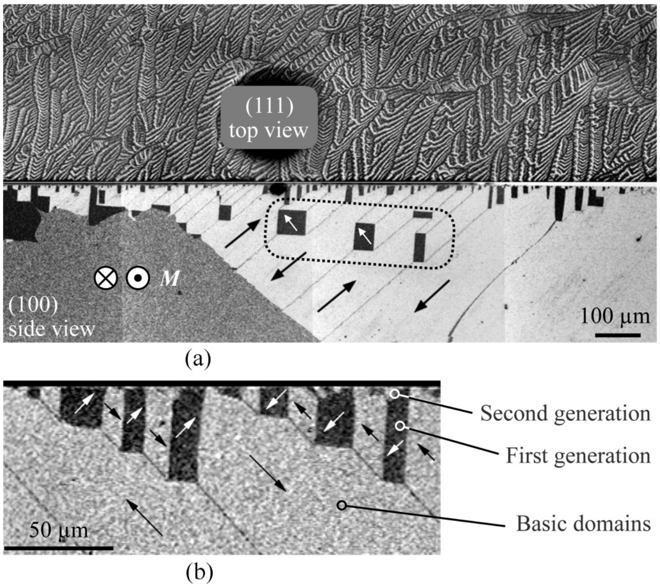

FIG. 17. (a) Top view and (100) side view of a Libovický crystal with (111) surface and a thickness of 1 mm. (b) High-resolution observation on a similar sample, showing two generations of echelons at the (111) surface. Image (b) is reprinted by permission from Ref. [16]. For a video of the frozen domains in an echelon crystal we refer to Supplemental Material [30].

are just branched up to two generations at most [Fig. 17(b)], independent of thickness. It seems that 90° walls, which are the basic components of the echelon domains, are disfavored compared to 180° walls. The extension of the echelons is therefore restricted to a narrow surface zone, while the bulk mostly consists of 180° domains. A domain coarsening in the direction of the volume takes place by built-in intermediate domains rather than by echelon iteration [in Fig. 17(b) such domains are marked by a dotted frame]. The reason for the discrimination of the 90° domains may be mechanical stress that is obviously present and active during the annealing of the FeSi crystals (see Supplemental Material [18]).

H. Grain boundary domains

To reveal the anatomy of "frozen" domains in a Libovický crystal, it has to be (possibly) cut, polished, and etched after precipitation annealing. Interestingly, we found that after polishing, but before etching, "life" domains can be imaged by Kerr microscopy even on a precipitated crystal — the precipitated microstructure has obviously no significant influence on the actual domains which behave like in a regular FeSi solid solution (no traces of an interaction between "life" and "frozen" domains were surprisingly identified). Of course the life domains differ from the frozen domains in detail, owing to different relative contributions of the magnetic energies at room temperature and at the annealing temperature and possibly by adapting to a different surface if the sample was cut. Nevertheless, valuable comparisons between the two domain types can be made.

This is demonstrated in Fig. 18 for a polycrystalline Fe 12.8 at.% Si sample. The crystal was 1-mm thick when it was annealed to freeze the domains. Then it was cut by half and the revealed central plane was carefully polished. The live domains on that plane were studied in the longitudinal Kerr effect at oblique incidence. Then the central plane surface was etched and the "frozen" domains at the same location were imaged, but at perpendicular incidence. This is the optimum condition for the birefrigence effect that is used to visualize the Libovický domains, while at the same time Kerr contrast is suppressed due to the typical in-plane magnetization of the FeSi material [31]. Note that the "frozen" domains are those present in the middle of the crystal during annealing, different to the "life" domains that adapt to the new surface.

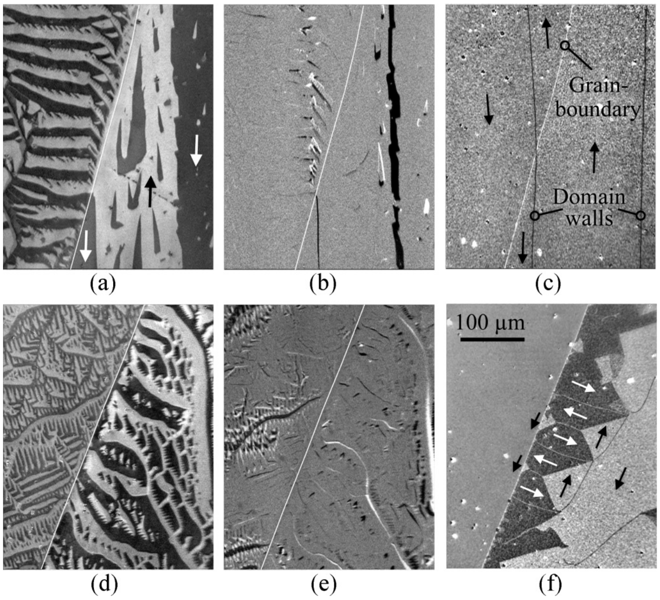

FIG. 18. Comparison of Kerr and Libovický observations around grain boundaries on the same polycrystalline Fe 12.8 at.% Si sample. All images are taken on the center plane of an originally 1-mm-thick crystal after cutting by half. (a, d) Kerr micrographs after AC demagnetization. (b, e) Difference images after applying a small magnetic field to the patterns in (a) and (d) with those patterns subtracted as reference images. (c, f) Frozen domains at the same sample locations as the corresponding Kerr images.

Two neighborhoods around grain boundaries were chosen. In Figs. 18(a) and 18(d) the "life" domains are shown after the sample was demagnetized in an applied AC magnetic field of decreasing amplitude. For Figs. 18(b) and 18(e) the domain states in Figs. 18(a) and 18(d) are subtracted as reference images from states with a small DC magnetic field applied. If the domains would not have changed, the difference images [Figs. 18(b) and 18(e)] would be without contrast. Any contrast in those images indicates domain changes relative to the reference states.

In terms of this difference image technique, the two grain boundaries in Fig. 18 reveal different characteristics: In the right grain in Fig. 18(b) a contrast shows up along the 180° walls. They obviously moved in the magnetic field compared to the state in Fig. 18(a). This wall motion seems to continue in the left grain, indicating that in the volume of this grain wide 180° domains are present, which are not seen in the surface domains in Fig. 18(a). The wall activity across the grain boundary suggests that this is a magnetically "soft" boundary, allowing for easy flux penetration by wall motion. This is different for the grain boundary in Figs. 18(d) and 18(e). According to the image in Fig. 18(e), there is domain activity in both neighboring grains, while in the direct neighborhood of the boundary the activity is blocked. So, this seems to be a magnetically "hard" boundary with reduced permeability for the flux. The "frozen" domains, shown in Figs. 18(c) and 18(f), confirm this finding: While across the grain boundary in Fig. 18(c) a 180° wall can indeed be seen, which was apparently present already in the bulk during annealing, a kind of closure domain structure was formed at the grain boundary in Fig. 18(f), which keeps the magnetic flux closed within the grain on the right.

From these observations we may conclude that it seems justified to assess the permeability of grain boundaries for magnetic flux transport by studying the domain activity on the *surface* of a polycrystalline sample. The surface domains are part of an underlying bulk domain network, so any domain activity in the volume is likely to act on the surface domains as nicely seen in the left grain of Fig. 18(b). Internal grain boundary domains, like those in Fig. 18(f) that block the flux, lead to a stiffening of the magnetization around the grain boundary that resembles itself also in a reduced surface domain activity. The hardness or softness of a grain boundary will depend on the relative orientation of easy axes on both sides of the boundary, the orientation of the boundary itself, and the direction of magnetic field. The example presented here is a first step to correlate surface observations by Kerr microscopy with bulk domain analysis — no attempt was made yet for a thorough, systematic analysis.

IV. SUMMARY

In this article a review is given on selected basis domain patterns in ironlike material, which are typically found in crystals with well-oriented and misoriented main surfaces. The anatomy of the patterns was studied by Libovický tomography and the results were compared with textbook models. The main results are the following.

(1) The existence of Néel spike domains around nonmagnetic inclusions in the bulk is proven for the first time. It is shown that large defects can have pinning effects on the whole domain wall network in their neighborhood.

(2) For slightly misoriented (100) surfaces a first-generation supplementary domain pattern, on which fir tree domains as a second-generation pattern are superimposed, is discovered. This possibility of multigeneration supplementary domains on slightly misoriented surfaces was overlooked in the past.

(3) The model for the V-line pattern on ideally oriented (100) surfaces, consisting of perpendicular basic domains and V-shaped closure domains at the surface, can be verified. The V-line pattern is always restricted to surface zones, while in the deeper bulk much wider basis domains are observed. Such a layered domain character is likely caused by the influence of layered mechanical stress.

(4) The conventional model for the supplementary moth pattern, found on slightly misoriented (100) surfaces with perpendicular basic domains, is disproved. Rather than being guided to the basic domains, the misorientation-induced perpendicular magnetic flux component appears to be closed within the V-shaped closure domains.

(5) The chain pattern, observed on ideally oriented (110) crystal surfaces, is confirmed to consist of spike and closure domains as expected from the model.

(6) The ant pattern, being part of stress pattern II on (110) related surfaces, is shown do disappear in a depth of some micrometers according to model predictions.

(7) On wedge crystals with extremely misoriented (111) surfaces the dependence of the bulk domain width on the crystal thickness is quantitatively analysed, finding a square-root dependency. This behavior is expected from theory and the given circumstance that multiple generations of echelon branching are suppressed in Libovický material.

(8) The combined observation of surface domain activity by Kerr microscopy and bulk domain analysis by Libovický tomography supports the idea of an experimental procedure to analyze the flux permeability of grain boundaries in polycrystalline material.

All domain patterns, presented in this article, were originally discovered by surface domain observation and their models were derived by using arguments from domain theory. The confirmation of the models by Libovický tomography creates confidence in the power of this combined approach and the relevance of surface domain observation for bulk material. This is also true for grain boundary effects in polycrystalline materials. The overlooking of phenomena, like those that were discovered here for the fir tree and moth patterns, cannot be excluded, though.

ACKNOWLEDGMENTS

The FeSi crystals were grown, oriented, and cut by G. Behr, A. Teresiak, and C. Götzel (all IFW), respectively. Thanks to Daniel Wolf (IFW) for helping to create sectional views, and to Ivan Soldatov (IFW) for valuable suggestions on the manuscript. This work was supported by the DFG through Grant No. SCHA726/1-1.

---

[1] A. Hubert and R. Schäfer, *Magnetic Domains: The Analysis of Magnetic Microstructures* (Springer, Berlin, 1998).

[2] G. T. Herman, *Fundamentals of Computerized Tomography: Image Reconstruction From Projection* (Springer, London, 2009).

[3] C. Donnelly and V. Scagnoli, J. Phys.: Condens. Matter **32**, 213001 (2020).

[4] R. Streubel, F. Kronast, P. Fischer, D. Parkinson, O. Schmidt, and D. Makarov, Nat. Commun. **6**, 7612 (2015).

[5] C. Donnelly, M. Guizar-Sicairos, V. Scagnoli, S. Gliga, M. Holler, J. Raabe, and L. Heyderman, Nature **547**, 328 (2017).

[6] C. Donnelly, S. Finizio, S. Gliga, M. Holler, A. Hrabec, M. Odstrčil, S. Mayr, V. Scagnoli, L. Heyderman, M. Manuel

Guizar-Sicairos, and J. Raabe, Nat. Nanotechnol. **15**, 356 (2020).

[7] D. Wolf, N. Biziere, S. Sturm, D. Reyes, T. Wade, T. Niermann, J. Krehl, B. Warot-Fonrose, B. Büchner, E. Snoeck, C. Gatel, and A. Lubk, Commun. Phys. **2**, 87 (2019).

[8] A. Lang, Acta Crystallogr. **12**, 249 (1959).

[9] J. Miltat, Philos. Mag. **33**, 225 (1976).

[10] C. Grünzweig, C. David, O. Bunk, M. Dierolf, G. Frei, G. Kühne, J. Kohlbrecher, R. Schäfer, P. Lejcek, H. M. R. Rønnow, and F. Pfeiffer, Phys. Rev. Lett. **101**, 025504 (2008).

[11] R. Harti, M. Strobl, R. Schäfer, N. Kardjilov, A. Tremsin, and C. Grünzweig, Sci. Rep. **8**, 15754 (2018).

[12] I. Manke, N. Kardjilov, R. Schäfer, A. Hilger, M. Strobl, M. Dawson, C. Grünzweig, G. Behr, M. Hentschel, C. David, A. Kupsch, A. Lange, and J. Banhart, Nat. Commun. **1**, 125 (2010).

[13] S. Libovický, Phys. Stat. Solidi A **12**, 539 (1972).

[14] H. Warlimont, Metallkunde **59**, 595 (1968).

[15] S. Schinnerling and R. Schäfer, Prakt. Metallogr. **37**, 501 (2000).

[16] R. Schäfer and S. Schinnerling, J. Magn. Magn. Mater. **215-216**, 140 (2000).

[17] S. Shin, R. Schäfer, and B. C. De Cooman, Metall. Mater. Trans. A **44**, 4239 (2013).

[18] See Supplemental Material at http://link.aps.org/supplemental/10.1103/PhysRevB.101.214430 for a discussion on the relevance of mechanical stress for the frozen domains in Libovický crystals.

[19] R. Schäfer, Investigation of domains and dynamics of domain walls by the magneto-optical Kerr-effect, in *Handbook of Magnetism and Advanced Magnetic Materials* (John Wiley and Sons, New York, 2007).

[20] W. Kuch, R. Schäfer, P. Fischer, and F. Hillebrecht, *Magnetic Microscopy of Layered Structures* (Springer, Berlin, 2015).

[21] L. Néel, Cahiers de Phys. **25**, 21 (1944).

[22] H. Williams, Phys. Rev. **71**, 646 (1947).

[23] H. Williams and W. Shockley, Phys. Rev. **75**, 178 (1949).

[24] L. Bates and D. Martin, Proc. Phys. Soc. B **69**, 145 (1956).

[25] L. Bates and R. Carey, Proc. Phys. Soc. **75**, 880 (1960).

[26] D. Ganz, Arch. Eisenhtten **35**, 371 (1964).

[27] See Supplemental Material at http://link.aps.org/supplemental/10.1103/PhysRevB.101.214430 for a video that displays all 87 individual images towards a depth of 68 μm.

[28] See Supplemental Material at http://link.aps.org/supplemental/10.1103/PhysRevB.101.214430 and http://link.aps.org/supplemental/10.1103/PhysRevB.101.214430 for videos that displays all 33 individual images towards a depth of 48 μm. The two videos were taken with 10x and 20x objective lenses, respectively.

[29] See Supplemental Material at http://link.aps.org/supplemental/10.1103/PhysRevB.101.214430 for a video that displays all 33 individual images towards a depth of 15 μm. For tomography, the sample was polished in steps of 0.25 μm down to a depth of 6 μm and then in steps of 1 μm down to the depth of 15 μm.

[30] See Supplemental Material at http://link.aps.org/supplemental/10.1103/PhysRevB.101.214430 for a video that displays the change of domains down to a depth of 150 μm.

[31] I. Soldatov and R. Schäfer, Rev. Scient. Instrum. **88**, 073701 (2017).